

# Wind Disturbance Rejection for an Insect-Scale Flapping-Wing Robot

Pakpong Chirarattananon<sup>1</sup>, Kevin Y. Ma<sup>2</sup>, Richard Cheng<sup>3</sup>, and Robert J. Wood<sup>2</sup>

**Abstract**—Despite having achieved unconstrained stable flight, the insect-scale flapping-wing robot is still tethered for power and control. Towards the goal of operating a biologically-inspired robot autonomously outside of laboratory conditions. In this paper, we simulate outdoor disturbances in the laboratory setting and investigate the effects of wind gusts on the flight dynamics of a millimeter-scale flapping wing robot. Simplified models describing the disturbance effects on the robot's dynamics are proposed, together with two disturbance rejection schemes capable of estimating and compensating for the disturbances. The proposed methods are experimentally verified. The results show that they reduced the root mean square position errors by approximately 50% when the robot was subject to  $60 \text{ cm}\cdot\text{s}^{-1}$  horizontal wind.

## I. INTRODUCTION

Foreseeable applications of small flying robots in our everyday lives, ranging from city courier services to automated aerial construction [1], have driven advances in research in the area of *Micro Aerial Vehicles* (MAVs) as seen in innumerable examples [1], [2], [3]. Among these, multi-rotor vehicles have gained considerable popularity thanks to simple mechanical designs and well-understood dynamic properties.

Biologically-inspired MAVs are another platform for active research [4], [5]. Flapping-wing devices are particularly of interest owing to their expected maneuverability exemplified by their natural counterparts. Inspired by tiny flying insects, researchers have developed and demonstrated stable unconstrained flight of an insect-scale robot (shown in figure 1) in [6], [7]. The results reflect the culmination of research in meso-scale actuation and manufacturing technology [6], [8], as well as understanding in control, stability, and aerodynamics of flapping flight [9], [10], [11].

Despite having achieved stable flight, the flapping-wing robot prototype in figure 1 is still tethered for power and control. Limited by the payload capacity (the robot can

This work was partially supported by the National Science Foundation (award number CCF-0926148), and the Wyss Institute for Biologically Inspired Engineering. Any opinions, findings, and conclusions or recommendations expressed in this material are those of the authors and do not necessarily reflect the views of the National Science Foundation.

<sup>1</sup>Pakpong Chirarattananon is with the Department of Mechanical and Biomedical Engineering, City University of Hong Kong, Hong Kong (email: pakpong.c@cityu.edu.hk).

<sup>2</sup>Kevin Y. Ma and Robert J. Wood are with the School of Engineering and Applied Sciences, Harvard University, Cambridge, MA 02138, USA, and the Wyss institute for Biologically Inspired Engineering, Harvard University, Boston, MA, 02115, USA (email: kevinma@seas.harvard.edu; rjwood@eecs.harvard.edu).

<sup>3</sup>Richard Cheng is with the Department of Mechanical and Aerospace Engineering, Princeton University, Princeton, NJ 08544, USA (email: rc-three@princeton.edu).

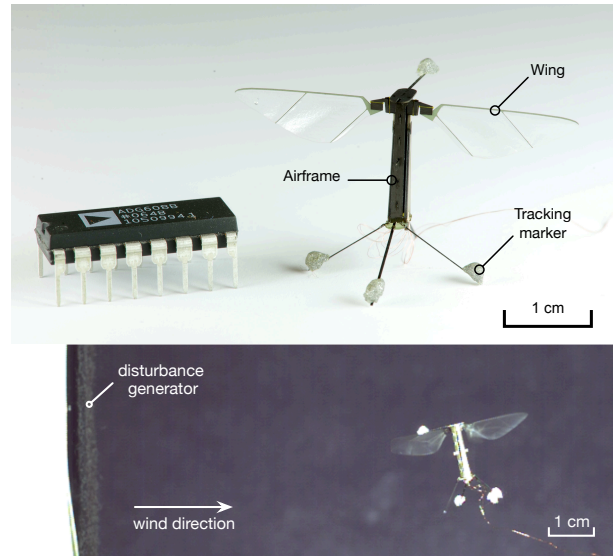


Fig. 1. (top) Photograph of a biologically-inspired robotic insect with four reflective markers for tracking purposes next to a 16-pin dual in-line package (DIP) integrated circuit for scale. (bottom) A still image of a flapping-wing robot flying in the presence of horizontal wind disturbance in the flight arena.

carry no more than 30 – 40 mg in addition to its current weight of 80 mg), sensing and control computation are executed offboard. A motion capture system provides real-time feedback on the position and orientation of the robot by triangulating the positions of four retro-reflective markers placed on the robot. Computed control signals are delivered to the robot via a four-wire tether.

Thus far, we have demonstrated hovering flight [7], basic flight maneuvers [11], and realization of an acrobatic pre-planned flight trajectory such as perching on a vertical surface [12]. In the meantime, research activities are being carried out to fly this vehicle autonomously outside of laboratory conditions. Alternative sensing devices with suitable power and mass have been explored, ranging from a micro-electromechanical inertial measurement unit [13] to the small footprint onboard vision sensor inspired by insect ocelli [14]. Lightweight and efficient power electronics have also been designed [15]. In preparation for outdoor operations, another important avenue of research is to investigate and overcome the effects of external disturbances such as wind on the flight stability of the robot.

To date, the effects of wind disturbances on MAVs have been studied in the context of rotary-wing and fixed-wing vehicles [2], [16], [17], [18]. In [2], [16], [17], wind disturbance were estimated and compensated for under various schemes

in the problem of position control of quadrotors. The proposed methods were verified in simulations. Nevertheless, the lack of experimental validation casts doubt on the accuracy of the aerodynamic models and the effects of turbulence flow on the vehicles. In another example [18], researchers tackle the wind disturbance problem for a fixed-wing MAV in an attempt to perch on a wire by experimentally characterizing the wind profile and elegantly designing an adaptive controller with verified regions of attraction. The strategies were then successfully tested in an outdoor environment. The effects of wind disturbances on flapping flight are different owing to unsteady aerodynamics. The topic of disturbances and forward flight has been mostly rudimentarily studied in real insects [9], [10], [19]. In this work, we seek to stabilize and control the position of an insect-scale flapping-wing robot in the presence of wind gusts by rejecting the disturbances based on simplified aerodynamic models.

First, we briefly cover the dynamic model of the robot. Based on previous work and preliminary results, we propose a simple model describing the effects of the wind disturbances on flight dynamics for flight control purposes. Two disturbance rejection strategies compatible with the existing flight controller and the proposed disturbance model are described. The two schemes are employed in the flight control experiments to stabilize the flapping-wing robot under the presence of  $60 \text{ cm}\cdot\text{s}^{-1}$  horizontal wind. Finally, experimental results are presented and discussed.

## II. MODELING OF ROBOT'S DYNAMICS AND THE EFFECTS OF WIND DISTURBANCES

### A. Robot Description and Dynamics

The flight-capable 80-mg flapping-wing robot in figure 1 was designed after its underactuated predecessor in [20]. The current prototype, with a wingspan of 3.5 cm, is fabricated using laser micro-machining and the *Smart Composite Microstructures* (SCM) process as detailed in [6]. Two piezoelectric bending actuators serve as flight muscles. When a voltage is applied across the piezoelectric plates, it induces approximately linear motion at the tip of the actuator, which is transformed into an angular wing motion by a spherical four-bar transmission. Each actuator is capable of independently driving a single wing. It turns out that mechanical properties of the coupled actuator-transmission-wing subsystems approximate that of a second-order linear system [21], roughly equivalent to an ideal forced mass-spring-damper system. The elastic potential energy of the bending actuator resembles the potential energy stored in a spring, while energy dissipated through aerodynamic drag on the wing parallels the loss in a damper. In operation, the robot is nominally driven with signals near the system's resonant frequency of 120 Hz to maximize the flapping stroke amplitude and minimize the reactive power expended by wing inertia. Lift is modulated by altering the amplitudes of the driving signals. Pitch, roll, and yaw torques are generated by appropriately modifying the nominal sinusoidal signals as described in [7]. The inherent instability of the

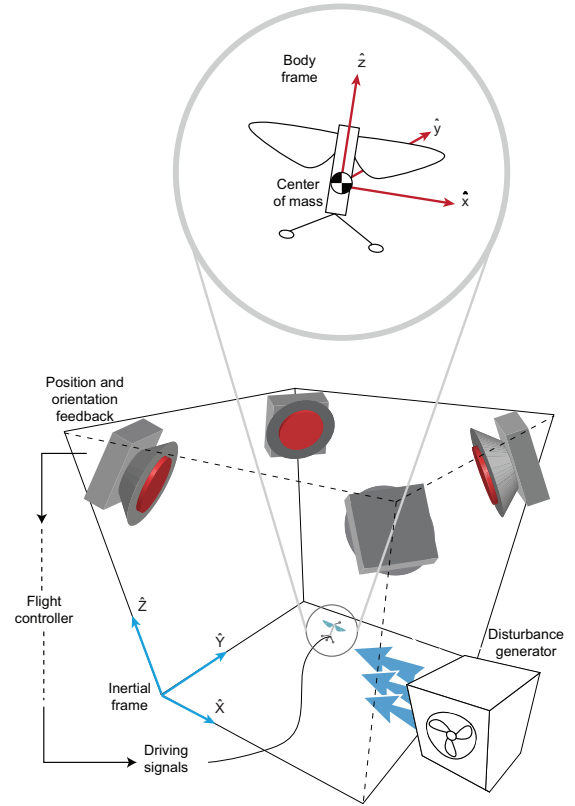


Fig. 2. A schematic diagram illustrating i) the flight arena equipped with 4-8 motion capture cameras for position and orientation feedback and ii) the definitions of the inertial frame and the body-attached frame.

system [9], [22], [23] necessitates real-time feedback control for the vehicle to achieve stable flight.

To describe the dynamics of the robot, we first define the inertial frame of reference  $(\hat{X}, \hat{Y}, \hat{Z})$  and the body-attached frame  $(\hat{x}, \hat{y}, \hat{z})$  as depicted in figure 2. A rotation matrix  $R$  (where  $R = \begin{bmatrix} \hat{x} & \hat{y} & \hat{z} \end{bmatrix}$ ) describes the relation between the two coordinate frames. In flight, the flapping motion creates the mass-normalized lift force  $(\Gamma)$  that nominally passes through the center of mass and aligns with the  $\hat{z}$ -axis of the robot. Additional aerodynamic damping force caused by external wind disturbances is denoted by a vector  $F_w$ . The resultant equation of motion describing the translational dynamics of the robot is given as

$$m\ddot{\mathbf{X}} = m\Gamma\hat{z} + m\mathbf{g} + F_w. \quad (1)$$

The rotational dynamics of the robot is given by Euler's equation:

$$\tau_c + \tau_w = J\dot{\omega} + \omega \times J\omega, \quad (2)$$

where  $\tau_c$  is a  $3 \times 1$  vector of torques generated by the flapping motion as commanded by the controller, and  $\tau_w$  represents the torque contributed by the effects of wind disturbances on the robot.

### B. Effects of Wind Disturbance

In this work, we assume that when the horizontally moving air encounters the robot, it gives rise to a drag force linearly

proportional to relative velocity. The linear assumption, as presented in [23], [10], is due to the dominant contribution from the interaction between the flapping wings and moving air. Empirical evidence suggests that this assumption is approximately valid for a flapping-wing robot at this scale for both head-on wind and lateral wind at low wind speed (less than  $1.5 \text{ m}\cdot\text{s}^{-1}$ ) [23]. By a similar argument, laterally moving air would also cause additional lift in the direction perpendicular to the drag (or along the  $\hat{z}$ -axis). As a result, we propose that the effects of wind disturbance on the translational dynamics of a flapping-wing robot can be described as

$$F_w = mb_x (\mathbf{v} \cdot \hat{x}) \hat{x} + mb_y (\mathbf{v} \cdot \hat{y}) \hat{y} + mb_z \|\mathbf{v} \times \hat{z}\| \hat{z}, \quad (3)$$

where  $\mathbf{v} = [v_x, v_y, 0]^T$  is a vector of relative air velocity. For a hovering or near-hovering robot,  $\mathbf{v}$  may be taken as the disturbance wind velocity. Equation (3) assumes different normalized damping coefficients ( $b_x, b_y, b_z$ ) for drag (and lift) along different body axes. Wind-tunnel experiments in [23] suggest that the values of  $b_x$  and  $b_y$  are comparable. The distinct structure of  $F_w$  along the  $\hat{z}$ -direction is owing to the mentioned lift, which is assumed to be a linear function of wind velocity on the  $\hat{x} - \hat{y}$  plane. Since  $F_w$  does not necessarily pass through the center of mass of the robot, it is anticipated to perturb the rotational dynamics of the robot as well. We model the torque contribution from the wind disturbance on the robot as the following

$$\tau_w = J \begin{bmatrix} -\beta_x (\mathbf{v} \cdot \hat{y}) & \beta_y (\mathbf{v} \cdot \hat{x}) & 0 \end{bmatrix}^T, \quad (4)$$

where  $\beta_x$  and  $\beta_y$  are corresponding rotational damping coefficients (normalized by the inertia  $J$ ). Equation (4) can be interpreted as the the product of  $F_w$  with appropriate effective moment arms and normalizing factors. The absence of torque along the  $\hat{z}$ -axis is based on an assumption regarding the symmetry of the robot and its nominal flapping motions. It is important to mention that equations (3) and (4) are modeled based on limited experimental evidence. While their validity is debatable, the primary goal is that they capture the dominant effects observed in the experiments and are sufficiently accurate for controller design purposes.

### III. CONTROL STRATEGIES

#### A. Adaptive Tracking Flight Controller

In this paper, we propose two wind disturbance rejection schemes and demonstrate how they can be implemented on the existing adaptive tracking flight controller, which is presented in [24]. For completeness, in this section we briefly describe the fundamental elements of the existing flight controller. The explanation on how the disturbance rejection components are integrated into the flight controller is given in section III-B.

The structure of the adaptive tracking flight controller in [24] is illustrated in a simplified schematic diagram in figure 3. The controller comprises of two primary components: a lateral controller and a altitude controller, operating in parallel.

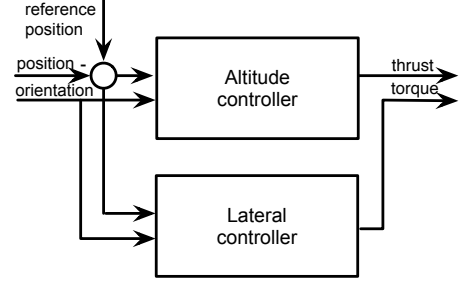


Fig. 3. A simplified block diagram showing the underlying structure of the adaptive tracking flight controller from [24]. The lateral controller operates in parallel with the altitude controller.

1) *Lateral controller*: The lateral controller computes the torque along three body axes (roll, pitch, and yaw) that the robot needs to produce in order to stabilize its attitude and follow the desired trajectory, given the current normalized thrust ( $\Gamma$ ) commanded by the altitude controller. In the first step, we define an error vector  $\mathbf{e}$  as a notion of the position error and its higher order derivatives, based on techniques borrowed from sliding mode control [25], as

$$\mathbf{e} = \mathbf{X}^{(3)} - \mathbf{X}_r^{(3)} + \lambda_1 (\ddot{\mathbf{X}} - \ddot{\mathbf{X}}_r) + \lambda_2 (\dot{\mathbf{X}} - \dot{\mathbf{X}}_r) + \lambda_3 (\mathbf{X} - \mathbf{X}_r), \quad (5)$$

where the subscript  $r$  denotes the reference trajectory, the bracketed superscript ( $i$ ) represents the  $i^{\text{th}}$ -order time derivative, and  $\lambda_i$ s are positive constants. The lateral controller is designed to minimize the projection of  $\mathbf{e}$  on the robot's pitch and roll axes, and the yaw rate ( $\omega_z$ ). In other words, we define a  $3 \times 1$  composite vector  $\mathbf{S}$  as  $\mathbf{S} = [-\Gamma^{-1} \mathbf{e} \cdot \hat{y} \quad \Gamma^{-1} \mathbf{e} \cdot \hat{x} \quad \omega_z]^T$ . The product of the moment of inertia matrix and the time derivative of  $\mathbf{S}$  yields the torque term and other parameters lumped into  $\Phi$ :

$$J\dot{\mathbf{S}} = \tau + \Phi. \quad (6)$$

The appearance of the torque term enables us to design a control law to manipulate the dynamics of  $\mathbf{S}$ . In the absence of external disturbances,  $\tau$  represents the torque generated by the robot. The controller is designed such that  $J\dot{\mathbf{S}} = -K\mathbf{S} - (\mathbf{S} \times J\omega)$ . As a result, for a Lyapunov function candidate  $V = \frac{1}{2} \mathbf{S}^T J \mathbf{S}$ , its time derivative  $\dot{V} = \mathbf{S}^T J \dot{\mathbf{S}} = -\mathbf{S}^T K \mathbf{S}$  is negative definite and the system is proven asymptotically stable.

When there are unknown quantities (for example, unknown torque offsets) in the system, adaptive components are incorporated to estimate those quantities, resulting in a modification to the Lyapunov function candidate. For the sake of simplicity, in this paper we assume that in the disturbance rejection experiments, these parameters have converged sufficiently close to their true values after prior flights. As a consequence, equation (6) and its corresponding Lyapunov analysis are presumed.

As outlined in section II-B, when present, wind disturbances affect the robot as a disturbance force and a disturbance torque as modeled by equations (3) and (4). In

order to stabilize the robot and ensure that the trajectory tracking ability is not compromised, we need to modify the flight controller accordingly.

Fortunately, the derivation of the lateral flight controller above (for the complete version, refer to [24]) does not explicitly rely on the translational dynamics (equation (1)).<sup>1</sup> The error vector  $\mathbf{e}$  is minimized when the robot perfectly follows the reference trajectory, independent of the existence of the disturbance force. On the other hand, the torque disturbance alters equation (6) by introducing the  $\tau_w$  term. This leaves the time derivative of the Lyapunov function as  $\dot{V} = -\mathbf{S}^T K \mathbf{S} + \mathbf{S}^T \tau_w$ , which is no longer guaranteed to be negative definite. This demands a disturbance rejection component to stabilize the lateral dynamics as shown later in section (III-B).

2) *Altitude controller*: While the altitude controller is presented and executed separately from the lateral controller, they operate in parallel and could be regarded as a single block in the diagram in figure 3. Here the altitude controller regulates altitude by controlling the thrust generated by the robot. To inspect the altitude dynamics, we project the translational dynamics from equation (1) along the  $\hat{Z}$ -axis,

$$\begin{aligned} \ddot{Z} &= \ddot{\mathbf{X}} \cdot [0 \ 0 \ 1]^T \\ &= \Gamma R_{33} - g + (F_w/m) \cdot [0 \ 0 \ 1]^T. \end{aligned} \quad (7)$$

It follows that the projection of  $F_w$  on the  $\hat{Z}$ -axis concerns the following terms:

$$\begin{aligned} b_x (\mathbf{v} \cdot \hat{x}) \hat{x} \cdot [0 \ 0 \ 1]^T &= -b_x R_{13} R_{33} v_x \\ b_y (\mathbf{v} \cdot \hat{y}) \hat{y} \cdot [0 \ 0 \ 1]^T &= -b_y R_{23} R_{33} v_y \\ b_z \|\mathbf{v} \times \hat{z}\| \hat{z} \cdot [0 \ 0 \ 1]^T &= b_z R_{33} \|\mathbf{v} \times \hat{z}\|. \end{aligned} \quad (8)$$

The first two terms involving  $b_x$  and  $b_y$  can be positive or negative, depending on the robot's orientation and the wind direction, whereas the last term is always positive when the robot is in flight. Preliminary experimental results indicate that lateral wind brings about a dramatic increase in lift, suggesting that the last term dominates, allowing us to neglect  $b_x$  and  $b_y$  terms. The problem can be simplified further by assuming the condition  $R_{13}, R_{23} \ll 1$ —that is, the robot remains near the upright orientation,

$$\begin{aligned} (F_w/m) \cdot [0 \ 0 \ 1]^T &\approx b_z R_{33} \left[ \|\mathbf{v}\|^2 \right. \\ &\quad \left. - (v_x R_{13} + v_y R_{23})^2 \right]^{\frac{1}{2}} \\ &\approx b_z R_{33} \|\mathbf{v}\| + \mathcal{O}(\epsilon^2) \\ &\approx b_z R_{33} \|\mathbf{v}\|, \end{aligned} \quad (9)$$

where  $\epsilon \approx R_{13}, R_{23}$ . When substituted back to equation (7), this yields

$$\ddot{z} = (\Gamma + b_z \|\mathbf{v}\|) R_{33} - g. \quad (10)$$

For a constant or slowly time-varying wind disturbance, the  $b_z \|\mathbf{v}\|$  term behaves identically to a constant offset to the

<sup>1</sup>This is true when the disturbance force is constant or slowly time-varying in the inertial frame.

generated thrust. This property makes the disturbance effects on the altitude dynamics easy to deal with by the current adaptive controller.

## B. Wind Disturbance Rejection Schemes

1) *Adaptive estimation*: One strategy to counteract wind disturbances is to fully embrace the constant or slowly time-varying wind assumption, and adaptively estimate this effect based on feedback. We first consider the effect of the torque disturbance on the lateral controller by expressing equation (4), which involves four unknown parameters: namely  $\beta_x, \beta_y, v_x$ , and  $v_y$ . While it is possible to adaptively estimate four parameters, we opt to reduce the number to two by assuming  $\beta_x = \beta_y = \beta$ . In this case, the damping coefficient  $\beta$  can be lumped with the wind parameters  $v_x$  and  $v_y$ , allowing them to be estimated together as

$$\begin{aligned} \tau_w &= J \begin{bmatrix} -R_{12} & -R_{22} \\ R_{11} & R_{21} \\ 0 & 0 \end{bmatrix} \begin{bmatrix} \beta v_x \\ \beta v_y \end{bmatrix} \\ &= JY \mathbf{a}, \end{aligned} \quad (11)$$

where we have defined a  $3 \times 2$  matrix  $Y$  and a  $2 \times 1$  vector of unknowns  $\mathbf{a}$  accordingly. Let the notations  $(\hat{\cdot})$  and  $(\tilde{\cdot})$  denote an estimated quantity and the estimation error (i.e.,  $\tilde{a} = \hat{a} - a$ ). In flight, we command the controller to compensate for the torque disturbance by countering it with its estimate in addition to the existing control law. The time derivative of the composite variable  $\mathbf{S}$  from section III-A.1 becomes

$$\begin{aligned} J\dot{\mathbf{S}} &= -K\mathbf{S} - (\mathbf{S} \times J\omega) + JY\mathbf{a} - JY\hat{\mathbf{a}} \\ &= -K\mathbf{S} - (\mathbf{S} \times J\omega) - JY\tilde{\mathbf{a}}. \end{aligned} \quad (12)$$

By re-defining the Lyapunov function candidate as  $V = \frac{1}{2}\mathbf{S}^T J\mathbf{S} + \frac{1}{2}\tilde{\mathbf{a}}^T \Lambda^{-1} \tilde{\mathbf{a}}$  for some positive diagonal gain matrix  $\Lambda$  and employing the adaptive law  $\dot{\hat{\mathbf{a}}} = \Lambda Y^T J^T \mathbf{S}$ , it can be shown that we recover the condition  $\dot{V} = -\mathbf{S}^T K \mathbf{S}$ . That is, stability is guaranteed in a Lyapunov sense.

A similar strategy could be implemented to cope with the disturbance term in the altitude dynamics in equation (10). Since the altitude controller, taken from [24], employed in this work already possesses the ability to adaptively estimate and compensate for constant thrust offsets, it benefits from the fact that the effect of the constant wind disturbance is identical to an unknown thrust offset. Essentially, we do not need to explicitly amend the altitude controller to tackle lateral wind, except for changing the adaptive gain to be sufficiently large in order for the estimates to converge quickly.

2) *Least-squares estimation*: While the adaptive estimation method is simple and easy to implement, it relies heavily on the assumption that the wind disturbance is constant or slowly time-varying. Hence, we propose an alternative approach that relaxes the constant assumption slightly, allowing the adaptive algorithm to capture, to some extent, the temporal structure of the wind disturbance. The proposed strategy resembles the adaptive estimation method in that it

first estimates the disturbance and applies a counteracting input to eliminate the effects from the disturbance.

To derive the LS estimator component for the lateral controller, we begin with the partial result from equation (12), but representing the  $JY\mathbf{a}$  term by  $\tau_w$ , such that  $J\dot{\mathbf{S}} = -K\mathbf{S} - (\mathbf{S} \times J\boldsymbol{\omega}) + \tau_w - \hat{\tau}_w$ . Here the controller applies the compensating torque  $\hat{\tau}_w$  based on the current estimate of  $\hat{\tau}_w$ . This equation can be re-arranged and applied a first-order low pass filter  $f_p = p/(s+p)$ , where  $s$  is a Laplace variable and  $p^{-1}$  is an associated time constant,

$$f_p \left\{ J\dot{\mathbf{S}} - K\mathbf{S} + (\mathbf{S} \times J\boldsymbol{\omega}) + \hat{\tau}_w \right\} = f_p \{ \tau_w \}. \quad (13)$$

Denote the quantity on the left hand side of equation (13), which is readily computable, as  $\Psi(t)$ . The right hand side of equation (13) can also be represented in the discrete-time domain,

$$f_p \{ \tau_w \} = \frac{1 - e^{-pT}}{1 - z^{-1}e^{-pT}} z^{-1} \tau_w, \quad (14)$$

where  $T$  is a discrete sampling time and  $z^{-1}$  denotes the delay operator. Combining equations (13) and (14), we obtain

$$\tau [t_{i-1}] = \frac{1}{1 - e^{-pT}} (\Psi [t_i] - e^{-pT} \Psi [t_{i-1}]), \quad (15)$$

where  $[t_i]$  is an index for the discrete time domain (i.e.,  $t_i - t_{i-1} = T$ ). The lumped estimates of wind parameters can be found by representing  $\tau$  as  $JY\mathbf{a}$ , similar to equation (11) as

$$\mathbf{a} [t_{i-1}] = \frac{Y^{-1} [t_{i-1}] J^{-1}}{1 - e^{-pT}} (\Psi [t_i] - e^{-pT} \Psi [t_{i-1}]). \quad (16)$$

To obtain the estimate of  $\hat{\mathbf{a}}$ , we assumes that  $\mathbf{a}$  may possess some temporal structure. This inspires us to estimate  $\mathbf{a}$  via a *finite impulse response* (FIR) filter as  $\hat{\mathbf{a}}[t_i] = \sum_{k=1}^N \sigma_k z^{-kn} \mathbf{a}[t_i]$ . Here,  $N$  is the filter length,  $k$  can be regarded as an arbitrary step size, and  $\sigma_k$ s are corresponding coefficients to be found. Then the algorithm for a standard least-squares estimator with an exponential forgetting factor ( $\gamma$ ) is used to determine  $\sigma$ s that minimize  $\int_{\delta}^t e^{-\gamma(t-\delta)} \|\mathbf{a}(s) - \hat{\mathbf{a}}(s)\|^2 d\delta$  [25]. The current estimate  $\hat{\mathbf{a}}(t)$  depends entirely on these  $\sigma$ 's and  $\mathbf{a}$ 's in the past. Since, this is an iterative algorithm,  $\sigma$ 's are updated every time step. The controller then compensates for the torque disturbances by projecting  $\hat{\mathbf{a}}$  back to the appropriate space as  $\hat{\tau}_w = JY\hat{\mathbf{a}}$ .

The same strategy applies to the altitude controller in an attempt to correct for the disturbance force on the altitude dynamics. To elaborate, the unknown offset  $b_z \|\mathbf{v}\|$  is treated as a single parameter using the FIR filter. That is, it may be written as a combination of its past values in the same way that  $\hat{\mathbf{a}}$  is estimated. In this case the least-square method is implemented without the need for projection. The complete derivation is omitted for brevity.

## IV. EXPERIMENTAL RESULTS

### A. Experimental Setup

Unconstrained flight experiments were performed in a flight arena equipped with 4-8 motion capture *VICON* cameras. They provide position and orientation feedback of the

robot at the rate of 500 Hz, covering a tracking volume of  $0.3 \times 0.3 \times 0.3$  m. Control algorithms were implemented on an xPC Target (*MathWorks*) environment and executed at the rate of 10 kHz for both input sampling and output signal generation. Signals are generated through a digital-to-analog converter, amplified, and then delivered to the robot through four 51-gauge copper wires.

Prior to the disturbance rejection experiments, the robots underwent an extensive characterization and trimming process. This started by a visual inspection of the wings' kinematics at various operating frequencies to identify the system's resonance frequency, symmetry, and flapping amplitudes. Open-loop trimming flights were performed to determine suitable driving signals or the *trimmed conditions* that allowed the robot to liftoff, ideally vertically, in short (<0.3 seconds) flights. With closed-loop feedback, a well-trimmed robot could stabilize in short hovering flights (5-10 seconds) which served as closed-loop trimming flights. In these flights, the adaptive algorithms continuously updated the estimates of the unknown parameters. Once they converged, the insect-scale robot was able to hover at a designated setpoint within a body length. In case of mechanical fatigue or any damages on the robot, which occurs regularly (the lifetime of flexure-based wing hinges, for example, are <10 minutes [26]), manual part replacements or repairs are sometimes possible. In such circumstances, the complete characterizing and trimming process has to be repeated.

### B. Wind Disturbance Generator

We constructed a low-speed wind disturbance generator from an array of nine 12V DC fans fitted in a  $15 \times 15 \times 20$  cm box, capable of creating wind disturbances in a horizontal plane. An Arduino combined with an amplification circuit were used to execute commands received from the xPC Target system. In steady state, the wind generator is able to consistently generate wind with the speed ranging from  $(20 - 100) \pm 2 \text{ cm}\cdot\text{s}^{-1}$  as verified by a hot-wire anemometer. The variation of the wind speed over the area of  $15 \times 15$  cm around the setpoint (at the setpoint height) is generally less than  $\pm 3 \text{ cm}\cdot\text{s}^{-1}$ .

### C. Flight Experiments with Constant Wind Disturbances

To investigate the effects of lateral wind disturbances on the flapping-wing robotic insect, we carried out a series of experiments with the disturbance generator programmed to produce constant  $60 \text{ cm}\cdot\text{s}^{-1}$  wind in steady state. The wind blew in the positive  $\hat{X}$  direction. In the first set of experiments (four flights), no disturbance rejection scheme was implemented. Then seven flights (three and four) were performed with the adaptive estimation scheme and the least-squares estimator. Lastly both schemes were tested together in three flights. In summary, four sets of experiments were performed.

The time-trajectory plots of all 14 flights are shown in figure 4(a), together with the averaged wind profile at the setpoints measured by a hot-wire anemometer from six trials.

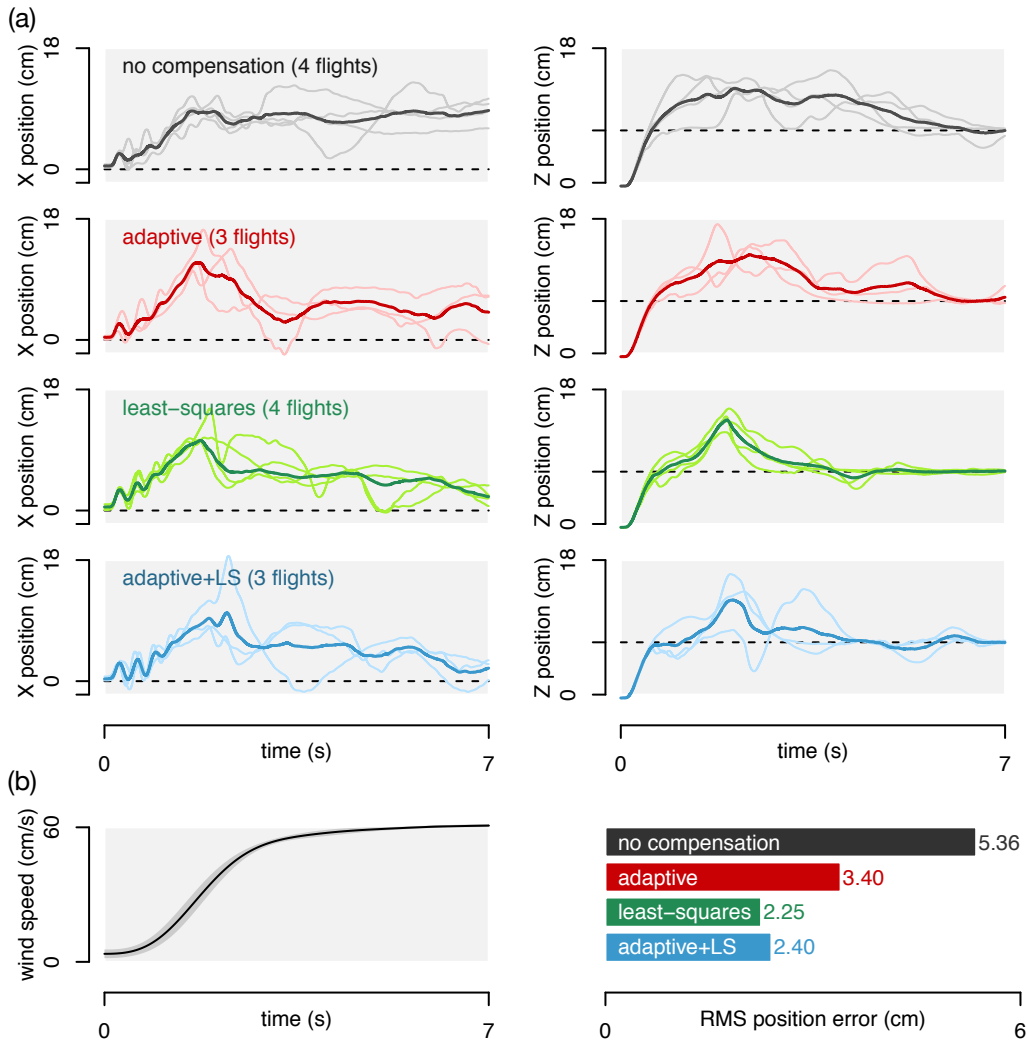


Fig. 4. (a) The plots show the trajectories obtained from the flight experiments with the wind disturbances blowing in the  $\hat{X}$ -direction. Light-colored lines represent individual flight trajectories and solid-colored lines represent the averaged trajectories from four experimental sets. (b) Left: the plot demonstrates the wind profile measured at the setpoint. Right: A bar graph compares the RMS position errors obtained from four experimental sets.

The time-dependency of the wind profile stems from the response time of the fans. Figure 4(a) reveals that without the disturbance rejection schemes (black lines), the robot gained significant altitude before it was blown and stayed at  $\approx 10$  cm away from the setpoint. At this position, the robot was able to maneuver back to the altitude setpoint.

The plots show that when the disturbance rejection schemes were in place, the initial part of the trajectory did not change significantly; Nevertheless, later on the robot managed to maneuver back to the setpoint to within a few centimeters in the  $\hat{X}$ -direction and a few millimeters in the  $\hat{Z}$ -direction. Quantitatively, we compare the performance of the proposed disturbance rejection schemes by computing the *root mean square* (RMS) values of the position error of the robot at the last second of flight ( $t = 6.0$  s to  $t = 7.0$  s) as shown in figure 4(b). The plot verifies that both proposed schemes significantly reduced the RMS error from the no compensation case. Particularly, when the least-

squares method was employed, the error decreased by more than 50%.

To better demonstrate the actual flight trajectory, we select one representative flight from the combined adaptive estimation and least-square estimation scheme. The 3D flight trajectory is reconstructed and presented in figure 5. The reconstruction confirms that the robot was initially blown away from the setpoint and gained excessive altitude before it recovered and came back towards the setpoint at the later phase of the flight. Footage of representative flights is available as a supplementary video.

## V. CONCLUSION AND DISCUSSION

In this paper, we study the effects of lateral wind disturbances on the flight of an insect-scale flapping-wing robot. The effects of wind disturbances on translational and rotational dynamics of the robot are simplified and modeled for control purposes. Based on a few simplifying assump-

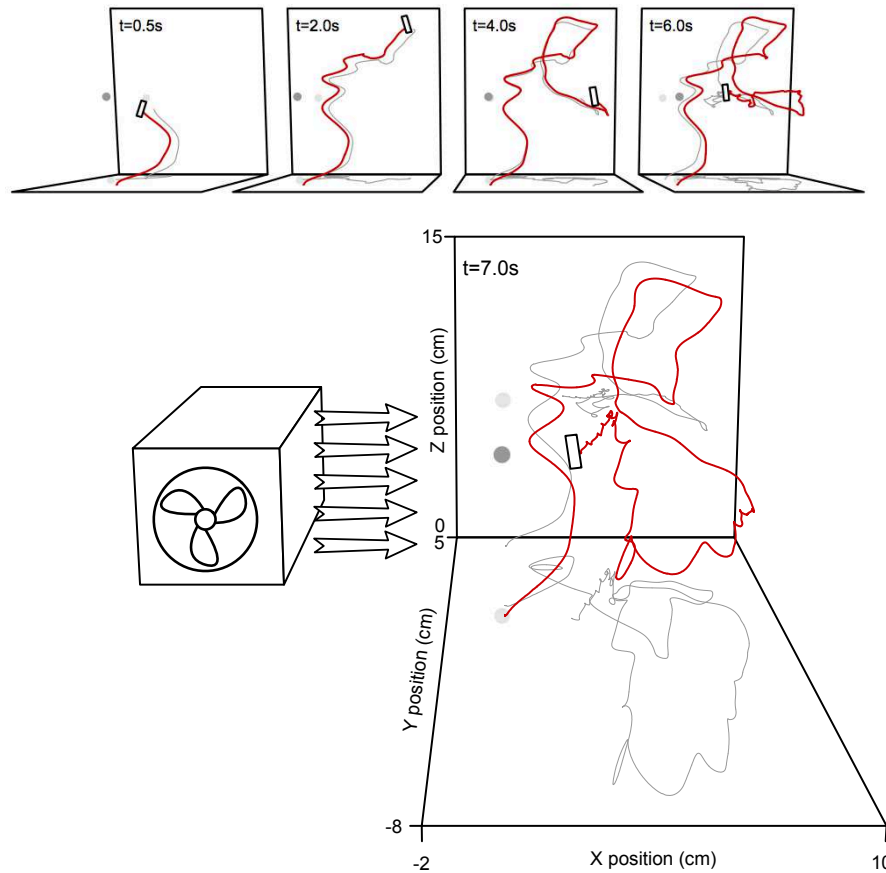


Fig. 5. (a) A 3D reconstruction of the robot’s trajectory during a 7-second hovering flight in the presence of  $60 \text{ cm}\cdot\text{s}^{-1}$  wind. Four sets of experiments were performed: i) with no compensation scheme, ii) with the adaptive estimation scheme, iii) with least-square estimation scheme, and iv) with the combined adaptive estimation and least-square estimation disturbance rejection schemes. Grey dots indicate the setpoint position and grey lines are projections on the wall and ground. (b) The averaged wind profile during 7-second flight and the RMS position error of the robot measured at the last one second of the flights.

tions, two disturbance rejection schemes compatible with the adaptive tracking flight controller previously developed in [24] are proposed. The strategies were implemented and verified in the flight control experiments.

The experimental findings bring several points for discussion. Without the rejection scheme, it can be seen that the robot initially gained considerably altitude and simultaneously it was blown away from the setpoint. This is qualitatively consistent with the proposed model in equation 3. Once the robot was further away from the lateral setpoint, it managed to maneuver back to the altitude setpoint. This is likely owing to the reduced wind speed further away from the disturbance generator.

Moreover, it is observed that the initial part of the trajectories when the disturbance rejection schemes were implemented does not differ from when the schemes were absent. This is due to the fact that the proposed schemes were not aware of the presence of the disturbance at the beginning and they require some time for the estimates to converge. This suggests that it is possible for the adaptive schemes to start with better initial guess of the estimates (in the experiments, they started by assuming no disturbance).

This avenue of research will be explored in future work.

Lastly, it is not entirely clear why the least-squares estimation scheme performed slightly better than the adaptive scheme. One possible explanation is the time variation of the wind profile in the actual experiments as shown in figure 4(b) as we expect the least-squares estimation method or the combined method may outperform the adaptive estimation approach as they take into account temporal variation. At this point, it is not conclusive to suggest whether the least-square scheme alone or the combined method is superior as the difference of their RMS errors is marginal and the sample size is too small to be statistically significant. It is anticipated that the difference could become evident with more experimental data (the sensitive and fragile nature of the robots severely limits the number of experiments and flight time). This will be further investigated in the future.

## REFERENCES

- [1] G. Hunt, F. Mitzalis, T. Alhinai, P. A. Hooper, and M. Kovac, “3d printing with flying robots,” in *Robotics and Automation (ICRA), 2014 IEEE International Conference on*, pp. 4493–4499, IEEE, 2014.

- [2] A. Mokhtari and A. Benallegue, "Dynamic feedback controller of euler angles and wind parameters estimation for a quadrotor unmanned aerial vehicle," in *Robotics and Automation, 2004. Proceedings. ICRA'04. 2004 IEEE International Conference on*, vol. 3, pp. 2359–2366, IEEE, 2004.
- [3] F. Bourgeois, L. Kneip, S. Weiss, and R. Siegwart, "Delay and dropout tolerant state estimation for mavs," in *Experimental Robotics*, pp. 571–584, Springer, 2014.
- [4] L. Daler, S. Mintchev, C. Stefanini, and D. Floreano, "A bioinspired multi-modal flying and walking robot," *Bioinspiration & biomimetics*, vol. 10, no. 1, p. 016005, 2015.
- [5] J. Gerdes, A. Holness, A. Perez-Rosado, L. Roberts, A. Greisinger, E. Barnett, J. Kempny, D. Lingam, C.-H. Yeh, H. A. Bruck, *et al.*, "Robo raven: A flapping-wing air vehicle with highly compliant and independently controlled wings," *Soft Robotics*, vol. 1, no. 4, pp. 275–288, 2014.
- [6] K. Y. Ma, S. M. Felton, and R. J. Wood, "Design, fabrication, and modeling of the split actuator microrobotic bee," in *Intelligent Robots and Systems (IROS), 2012 IEEE/RSJ International Conference on*, pp. 1133–1140, IEEE, 2012.
- [7] K. Y. Ma, P. Chirarattananon, S. B. Fuller, and R. J. Wood, "Controlled flight of a biologically inspired, insect-scale robot," *Science*, vol. 340, no. 6132, pp. 603–607, 2013.
- [8] J. Gafford, S. Kesner, R. Wood, and C. Walsh, "Microsurgical devices by pop-up book mems," *ASME Paper No. DETC2013-13086*, 2013.
- [9] I. Faruque and J. S. Humbert, "Dipteran insect flight dynamics, part 1 longitudinal motion about hover," *Journal of Theoretical Biology*, vol. 264, no. 2, pp. 538–552, 2010.
- [10] L. Ristroph, A. J. Bergou, J. Guckenheimer, Z. J. Wang, and I. Cohen, "Paddling mode of forward flight in insects," *Physical Review Letters*, vol. 106, no. 17, p. 178103, 2011.
- [11] P. Chirarattananon, K. Y. Ma, and R. J. Wood, "Adaptive control of a millimeter-scale flapping-wing robot," *Bioinspiration & Biomimetics*, vol. 9, no. 2, p. 025004, 2014.
- [12] P. Chirarattananon, K. Y. Ma, and R. J. Wood, "Fly on the wall," in *Biomedical Robotics and Biomechanics (2014 5th IEEE RAS & EMBS International Conference on*, pp. 1001–1008, IEEE, 2014.
- [13] S. B. Fuller, E. F. Helbling, P. Chirarattananon, and R. J. Wood, "Using a MEMS gyroscope to stabilize the attitude of a fly-sized hovering robot," in *IMAV 2014: International Micro Air Vehicle Conference and Competition 2014, Delft, The Netherlands, August 12-15, 2014*, Delft University of Technology, 2014.
- [14] S. B. Fuller, M. Karpelson, A. Censi, K. Y. Ma, and R. J. Wood, "Controlling free flight of a robotic fly using an onboard vision sensor inspired by insect ocelli," *Journal of The Royal Society Interface*, vol. 11, no. 97, p. 20140281, 2014.
- [15] M. Lok, D. Brooks, R. Wood, and G.-Y. Wei, "Design and analysis of an integrated driver for piezoelectric actuators," in *Energy Conversion Congress and Exposition (ECCE), 2013 IEEE*, pp. 2684–2691, IEEE, 2013.
- [16] S. L. Waslander and C. Wang, "Wind disturbance estimation and rejection for quadrotor position control," in *AIAA Infotech@ Aerospace Conference and AIAA Unmanned... Unlimited Conference, Seattle, WA, 2009*.
- [17] J. Escareño, S. Salazar, H. Romero, and R. Lozano, "Trajectory control of a quadrotor subject to 2D wind disturbances," *Journal of Intelligent & Robotic Systems*, vol. 70, no. 1-4, pp. 51–63, 2013.
- [18] J. L. Moore, *Robust post-stall perching with a fixed-wing UAV*. PhD thesis, Massachusetts Institute of Technology, 2014.
- [19] S. B. Fuller, A. D. Straw, M. Y. Peek, R. M. Murray, and M. H. Dickinson, "Flying drosophila stabilize their vision-based velocity controller by sensing wind with their antennae," *Proceedings of the National Academy of Sciences*, vol. 111, no. 13, pp. E1182–E1191, 2014.
- [20] N. O. Pérez-Arancibia, K. Y. Ma, K. C. Galloway, J. D. Greenberg, and R. J. Wood, "First controlled vertical flight of a biologically inspired microrobot," *Bioinspiration & Biomimetics*, vol. 6, no. 3, p. 036009, 2011.
- [21] B. M. Finio, N. O. Pérez-Arancibia, and R. J. Wood, "System identification and linear time-invariant modeling of an insect-sized flapping-wing micro air vehicle," in *Intelligent Robots and Systems (IROS), 2011 IEEE/RSJ International Conference on*, pp. 1107–1114, IEEE, 2011.
- [22] N. Gao, H. Aono, and H. Liu, "Perturbation analysis of 6DoF flight dynamics and passive dynamic stability of hovering fruit fly drosophila melanogaster," *Journal of theoretical biology*, vol. 270, no. 1, pp. 98–111, 2011.
- [23] S. B. Fuller, Z. E. Tech, P. Chirarattananon, N. O. Pérez-Arancibia, J. Greenberg, and R. J. Wood, "Stabilizing air dampers for insect-scale hovering aerial robots: An analysis of nonlinear dynamics based on flight tests gives design guidelines," 2015. under review.
- [24] P. Chirarattananon, K. Y. Ma, and R. J. Wood, "Single-loop control and trajectory following of a flapping-wing microrobot," in *Robotics and Automation (ICRA), 2014 IEEE International Conference on*, pp. 37–44, IEEE, 2014.
- [25] J.-J. E. Slotine, W. Li, *et al.*, *Applied nonlinear control*, vol. 60. Prentice-Hall Englewood Cliffs, NJ, 1991.
- [26] R. Malka, A. L. Desbiens, Y. Chen, and R. J. Wood, "Principles of microscale flexure hinge design for enhanced endurance," in *Intelligent Robots and Systems (IROS 2014), 2014 IEEE/RSJ International Conference on*, pp. 2879–2885, IEEE, 2014.